N-linked glycosylation enhances hemagglutinin stability in avian H5N6 influenza virus to promote adaptation in mammals

Honglei Sun[a,1,*], Guojing Deng[a,1], Haoran Sun[a,1], Jingwei Song[a,1], Wei Zhang[b,1], Han Li[a], Xiaohui Wei[a], Fangtao Li[a], Xin Zhang[a], Jiyu Liu[a], Juan Pu[a], Yipeng Sun[a], Qi Tong[a], Yuhai Bi[b], Yufeng Xie[b,c], Jianxun Qi[b], Kin-Chow Chang[d], George Fu Gao[b,e,f], Jinhua Liu[a,*]

[a]Key Laboratory of Animal Epidemiology and Zoonosis, Ministry of Agriculture, College of Veterinary Medicine, China Agricultural University, Beijing 100193, China; [b]CAS Key Laboratory of Pathogenic Microbiology and Immunology, Institute of Microbiology, Chinese Academy of Sciences (CAS), Beijing 100101, China; [c]Department of Basic Medical Sciences, School of Medicine, Tsinghua University, Beijing 100084, China; [d]School of Veterinary Medicine and Science, University of Nottingham, Sutton Bonington Campus, Loughborough, LE12 5RD, United Kingdom; [e]Chinese National Influenza Center, National Institute for Viral Disease Control and Prevention, Chinese Center for Disease Control and Prevention (China CDC), Beijing 102206, China; [f]WHO Collaborating Center for Reference and Research on Influenza, Beijing 102206, China.

[1] H.S., G.D., H.S., J.S., and W.Z. contributed equally to this work.

* Corresponding author. Jinhua Liu and Honglei Sun.

E-mail: Jinhua Liu: ljh@cau.edu.cn; Honglei Sun: shlei668@163.com

Keywords: H5N6 avian influenza virus; hemagglutinin; N-glycosylation; protein stability; mammalian adaptation; endosomal membrane fusion; zoonosis

Abstract

Clade 2.3.4.4 avian H5Ny viruses, namely H5N2, H5N6, and H5N8, have exhibited unprecedented intercontinental spread in poultry. Among them, only H5N6 viruses are frequently reported to infect mammals and cause serious human infections. In this study, the genetic and biological characteristics of surface hemagglutinin (HA) from clade 2.3.4.4 H5Ny avian influenza viruses (AIVs) were examined for adaptation in mammalian infection. Phylogenetic analysis identified an amino acid (AA) deletion at position 131 of HA as a distinctive feature of H5N6 virus isolated from human patients. This single AA deletion was found to enhance H5N6 virus replication and pathogenicity *in vitro* and in mammalian hosts (mice and ferrets) through HA protein acid and thermal stabilization that resulted in reduced

pH threshold from pH 5.7 to 5.5 for viral-endosomal membrane fusion. Mass spectrometry and crystal structure revealed that the AA deletion in HA at position 131 introduced an N-linked glycosylation site at 129 which increases compactness between HA monomers thus stabilizes the trimeric structure. Our findings provide a molecular understanding of how HA protein stabilization promotes cross-species avian H5N6 virus infection to mammalian hosts.

Significance Statement

Clade 2.3.4.4 H5N6 AIVs can cause serious human infection but the molecular basis of cross-species virus infection hitherto remains unknown. The viral surface glycoprotein HA is a major determinant of host tropism, pathogenicity and transmission. Here, we found that a point AA deletion (position 131) in the head of H5N6 virus HA generates a new N-linked glycosylation site at position 129 that lowers the pH threshold for membrane fusion, increases HA acid and thermal stability, thus promoting adaptation of H5N6 virus in mammalian hosts. Our findings show that N-linked glycosylation in HA affects viral fitness by influencing HA protein stability; thus, continual monitoring of circulating H5N6 virus for enhanced HA stability is prudent for pandemic preparedness.

MAIN TEXT

Introduction

AIVs continue to pose serious threats to poultry production and public health across the world. Highly pathogenic avian influenza (HPAI) H5 viruses have spread to more than 60 countries since the first report in 1996 (1). To date, H5 viruses have caused 939 recorded human infection cases (864 cases with H5N1 and 75 cases with H5N6) in 18 countries (2). The absolute number of human cases of H5 virus infection remains low. However, considering the global prevalence of H5 HPAI viruses and their tendency to mutate, there is a distinct possibility that given time they will acquire human-to-human transmissibility, either by mutational adaptations or through reassortment with other viruses (3-5). Since human populations lack immunity to A/H5 virus (6, 7), once an A/H5 virus gained human transmissibility, it could cause widespread human infections and even a pandemic.

Based on the HA gene of H5 viruses, 10 distinct phylogenetic clades (clades 0 to 9) have been identified. Clade 2.3.4 H5N1 viruses emerged in chickens and waterfowls in southern China in 2005 and have become predominant in Southeast Asia (8). Since 2010, its subclade 2.3.4.4 H5 reassortants, including H5N1, H5N2, H5N5, H5N6 and H5N8 viruses, have been frequently found in waterfowl and terrestrial poultry in Asian countries (9-12). Among these

H5Ny reassortants, H5N2, H5N6 and H5N8 are the dominant subtypes and have been disseminated by migratory birds to multiple countries across continents (13). Theoretically, these three virus subtypes are expected to have similar likelihood to infect humans. However, most confirmed human cases of clade 2.3.4.4 H5Ny virus infection were caused by H5N6 viruses (2), with the exception of human cases of H5N8 virus infection in Russia in 2021 (14). Since China reported the first human case of H5N6 virus infection in 2014, 75 H5N6 human cases have been documented, of which 32 (43%) were fatal (2). It is noteworthy that in 2021 alone, 38 new cases were reported, which further emphasizes the threat of cross-species transmission of H5N6 virus from birds to humans. Besides humans, H5N6 virus has also been isolated from other mammals, such as cats and pigs (15, 16). Increasing human and mammalian cases of severe H5N6 virus infections also indicate that this subtype could be a growing threat to public health. Therefore, understanding the molecular basis of its adaptation in mammals is critical for the control and prevention of H5 AIV infection in humans.

The viral surface glycoprotein HA, a trimeric class I membrane protein that binds sialic acid (SA)-containing receptors to initiate infection, is a major determinant of host tropism, pathogenicity and transmission (17). HA proteins of AIVs preferentially bind α-2,3 linked SA, and human-adapted viruses have a higher binding affinity for α-2,6 linked SA (18). Within minutes upon endocytosis, virions are exposed to increasing endosomal acidification. Upon reaching a pH threshold, typically ranging from pH 4.8 to 6.2 for different viruses, the spring-loaded HA "nanomachines" are triggered to undergo an irreversible conformational change and fuse viral envelope with the endosomal membrane (19). Generally, the pH values required for HA activation of AIVs are higher than those of human-derived influenza viruses (17). Thus, entry of IAV is regulated by HA receptor binding specificity and HA acid-stability. Previous work has shown that stabilized HA (pH < 5.6) and human-like receptor-binding preference in tandem are necessary for airborne transmission of A/H5 influenza virus between ferrets (4, 5). Furthermore, a stable HA protein has also been linked to pH1N1 pandemic potential and adaptation to humans (20, 21). At present, it remains unclear why the H5N6 virus subtype appears more likely to infect humans compared with other subtypes of clade 2.3.4.4 viruses. The role played by H5N6 virus HA in human and mammalian infection is also not clear.

In this study, we identified key functional differences in HA proteins of clade 2.3.4.4 H5Ny viruses and showed that the introduction of N-linked glycosylation at position 129 in the H5N6 HA protein lowered the activation threshold pH for membrane fusion from 5.7 to

5.5, and enhanced the structural stability of HA thus promoting cross-species transmission from birds to mammals.

Results

Predominance of a single amino acid deletion in the HA of H5N6 viruses isolated from human patients

Despite widespread distribution of clade 2.3.4.4 H5N2, H5N6 or H5N8 viruses in poultry populations, so far only the H5N6 subtype is known to have frequently infected humans and mammals. 75 human cases of H5N6 virus infection have been recorded to date (2), from which 28 genome sequences have been ascertained. To understand the genomic characteristics of clade 2.3.4.4 H5Ny viruses, we performed phylogenetic analysis of HA genes from H5N6, H5N8 and H5N2 viruses isolated in China. HA phylogeny identified four lineages in clade 2.3.4.4 viruses: H5N2, H5N8, Major H5N6 and Minor H5N6, and has been further subdivided into sublineages from "a" to "h" and H5N6 viruses have been assigned to various sublineages (SI Appendix, Fig. S1A). Notably, 20 out of 28 human H5N6 viruses were in the Major lineage (SI Appendix, Fig. S1B). All 28 human H5N6 isolates shared the similar molecular characteristics of HA with those of clade 2.3.4.4 H5Ny viruses, such as at the cleavage site and receptor-binding site (RBS). Interestingly, 16 out of the 28 (57.14%) human H5N6 isolates had an amino acid (AA) deletion at position 131 in the HA protein (131△, H3 numbering); in contrast, only 11% (80 out of 762) of avian H5N6 isolates harbored this deletion (SI Appendix, Fig. S1B). Further analysis showed that the HA 131△ was only found in the H5N6 subtype; no HA 131△ was found in H5N2 and H5N8 viruses (SI Appendix, Fig. S1C). Thus, an AA deletion at position 131, located at the head region of HA, is a viral feature associated with human cases of H5N6 virus infection.

131△ in HA enhanced viral replication and pathogenicity of avian H5N6 virus in mammalian hosts

To assess possible function of HA 131△ in H5N6 virus, a reverse-genetics derived H5N6 virus A/duck/Northern China/22/2017 (NC22/17-HA 131△) with HA 131△, and another virus with HA-131E (NC22/17-HA 131E) in the NC22/17 virus background were generated. Multistep replication kinetics of H5N6 virus NC22/17-HA 131△, and NC22/17-HA 131E were performed with a multiplicity of infection (MOI) of 0.001 in normal human bronchial epithelial cells (NHBE) and immortalized lung epithelial cells (A549) over 72 h. In NHBE cells, H5N6 virus NC22/17-HA 131△ replicated to significant higher levels than NC22/17-HA 131E from 24 to 72 h post-infection (hpi) ($P < 0.05$) (SI Appendix, Fig. S2A).

In A549 cells, progeny virus output of NC22/17-HA 131△ was about 10-fold higher than those of NC22/17-HA 131E virus between 36 and 72 h post-infection (hpi) ($P < 0.05$) (SI Appendix, Fig. S2B). Thus, 131△ in HA increased replication of H5N6 virus in human airway cells and may contribute to the fitness of H5N6 virus in humans.

Next, we evaluated the replication and pathogenicity of the two reassortant H5N6 viruses in BALB/c mice and ferrets. Mice intranasally (i.n.) inoculated with 10^6 median tissue culture infectious dose ($TCID_{50}$) of H5N6 virus NC22/17-HA 131△ exhibited severe symptoms, with a mortality of 80% (Fig. 1A). In contrast, no clinical signs were observed in mice inoculated with the same dose of H5N6 virus NC22/17-HA 131E during the 14-day period and all mice survived. Moreover, NC22/17-HA 131△ exhibited a 50% mouse lethal dose (MLD_{50}) value of $10^{5.625}$ $TCID_{50}$, while NC22/17-HA 131E virus being less pathogenic in mice had an MLD_{50} value $>10^{6.5}$ $TCID_{50}$ (Fig. 1A). Viral titers of NC22/17-HA 131△ in nasal turbinate were significantly higher than those of NC22/17-HA 131E virus at 3 and 5 day post-infection (dpi) ($P < 0.01$) (Fig. 1B). Histologically, mock-infected and NC22/17-HA 131E virus-infected nasal turbinates appeared normal; in contrast, NC22/17-HA 131△ virus-infected nasal turbinates contained erythrocytes and inflammatory cells adherent to the nasal mucosa, exhibited mild suppurative rhinitis. Mild bronchitis was found in NC22/17-HA 131E virus infected lungs, while NC22/17-HA 131△ virus-infected lungs exhibited severe peribronchiolitis and bronchopneumonia. No lesion was found in mock infected mice lung. Immunohistochemistry (IHC) staining also detected more viral antigen-positive cells in the nasal turbinates and lungs of mice infected with NC22/17-HA 131△ virus, compared with NC22/17-HA 131E virus. No viral antigen was observed in nasal turbinates and lungs of mock-infected mice (Fig. 1C).

Ferrets (*Mustela putorius furo*) are good animal models to study influenza virus infection as they exhibit clinical symptoms similar to humans. Three groups of ferrets (n = 3) were individually inoculated i.n. with 10^6 $TCID_{50}$ of each virus or PBS, and all animals were euthanized on 4 dpi for virus titration and histopathological examination. Ferrets infected with the NC22/17-HA 131E virus showed no obvious clinical symptoms, apart from transient temperature elevation at 2 dpi. In contrast, ferrets infected with NC22/17-HA 131△ virus exhibited clear clinical signs, including wheezing and coughing. NC22/17-HA 131△ virus titers were significantly higher ($P < 0.01$) in the nasal turbinates, tracheae, and lung tissues than in corresponding tissues of NC22/17-HA 131E virus infection (SI Appendix, Fig. S3A). Histopathology of H5N6 virus infection in ferrets were consistent with clinical signs. NC22/17-HA 131E virus-infected nasal turbinates showed some loss of epithelial cells; those

from NC22/17-HA 131△ virus infection, however, showed extensive erosion of mucous epithelia accompanied by the presence of inflammatory cells, indicating severe suppurative rhinitis. Lungs of NC22/17-HA 131E virus infection appeared normal, but those from NC22/17-HA 131△ virus infection exhibited severe bronchopneumonitis and localized interstitial pneumonia. No lesions were observed in organs of control ferrets. Additionally, viral-antigen-positive cells were more abundant in H5N6 NC22/17-HA 131△ virus infected tissues. No viral antigens were detected in organs of control ferrets (SI Appendix, Fig. S3B). Taken together, 131△ in HA of H5N6 virus confers increased viral replication, in particular in the upper respiratory tract (URT), and elevated pulmonary pathogenicity in mice and ferrets.

HA 131△ in avian H5N6 virus did not affect virus binding affinity for avian- and human-type SA receptors

Binding specificity of HA receptor is a critical determinant for cross-species transmission of influenza A viruses (22). HA mutations in the RBS and loss of the glycosylation site at residue 158 in clade 2.3.4.4 H5Ny viruses were found to confer increased affinity for human-like SAα2,6Gal receptor without affecting binding affinity for avian-like SAα2,3Gal receptor (23). Thus, we determined whether the HA 131△, located in the RBS region, could affect the receptor-binding properties of H5N6 viruses. Direct binding assays with SAα2,3Gal and SAα2,6Gal sialylglycopolymers were performed on four clade 2.3.4.4 H5Ny isolates (A/duck/Eastern China/30/2010 [EC30/10, H5N2]; A/duck/northern China/08/2014 [NC08/14, H5N8]; A/duck/eastern China/11/2014 [EC11/14, H5N6] with HA-131E; and wild type H5N6 virus NC22/17, with HA 131△) along with the two reverse-genetically derived H5N6 viruses, NC22/17-HA 131△ and NC22/17-HA 131E. A 2009 pandemic H1N1 virus A/Beijing/21/2019 (BJ21/19) and a clade 2.3.4 avian H5N1 virus A/duck/Anhui/01/2006 (AH01/06) were used as controls for preferential binding to SAα2,6Gal and SAα2,3Gal receptors, respectively. We found that all the four H5Ny viruses, NC22/17-HA 131△ and NC22/17-HA 131E viruses bound both SAα2,6Gal and SAα2,3Gal receptors with comparable affinity. In contrast, BJ21/19-H1N1 specifically bound to the human receptor, and AH01/06-H5N1 preferentially bound to the avian receptor (SI Appendix, Fig. S4A).

The affinity of the viruses for SAα2,6Gal-linked receptor was further assessed on human tracheal sections. All the four H5Ny viruses, NC22/17-HA 131△ and NC22/17-HA 131E viruses were able to bind tracheal epithelial cells at similar levels, further demonstrating their comparable potential to infect humans (SI Appendix, Fig. S4B). These data demonstrate that

HA 131△ mutation did not affect the receptor binding of H5N6 virus, and that clade 2.3.4.4 H5Ny viruses showed similar affinity for avian-type and human-type SA receptors.

HA 131△ in clade 2.3.4.4 H5N6 virus increases HA stability

Acid and thermal stability of HA protein has emerged as an important determinant in host range, transmissibility and pandemic potential of influenza viruses (17, 24). We evaluated the acid stability of HA 131△ mutant. A selection of clade 2.3.4.4 H5Ny viruses (EC30/10-H5N2, NC08/14-H5N8, EC11/14-H5N6 with HA-131E, and wild type H5N6 NC22/17 with HA 131△) were used in syncytia formation assays; human influenza virus BJ21/19-H1N1 (acid stable) and avian virus AH01/06-H5N1 (acid unstable) were used as controls. Vero cells infected with different viruses were incubated in buffers across a pH range between 5.0 and 6.0 to examine syncytia formation. The pH at which 50% maximum syncytia formation was regarded as the fusion pH. The fusion pH of EC30/10-H5N2, NC08/14-H5N8, EC11/14-H5N6 avian viruses were around 5.7-5.8, similar to or higher than that of avian virus AH01/06-H5N1 (pH 5.7) (Fig. 2A). On the other hand, wild type H5N6 NC22/17 virus had a fusion pH value of 5.5, and that of BJ21/19-H1N1 human virus was ≤ 5.2 (Fig. 2A). We found that NC22/17-HA 131△ virus effectively mediated syncytium formation at pH 5.5, while the fusion pH of NC22/17-HA 131E virus was higher at 5.7, similar to those of H5N2, H5N8 and early epidemic H5N6 viruses (Fig. 2A), indicating that 131△ affected the stability of HA protein by lowering its activation pH.

The conformational change of HA from a metastable non-fusogenic state to a stable fusogenic state can also be triggered at neutral pH when the HA is exposed to increasing temperature (25). To test HA thermostability, 128 hemagglutination units (HAUs) of each virus were incubated at 50℃ over a 14-hour time course, during which HA titers were determined every two hours. Consistent with the fusion pH findings, thermostability of EC30/10-H5N2, NC08/14-H5N8 and EC11/14-H5N6 viruses were similar to that of AH01/06-H5N1 avian virus, and the thermostability of H5N6 NC22/17 virus was similar to that of BJ21/19-H1N1 human virus (Fig. 2B). NC22/17-HA 131E virus showed a significant decrease in the HA titer after 4 h of incubation and exhibited no HA activity after 8 h. However, HA activity of NC22/17-HA 131△ virus was maintained throughout the entire 14 h of incubation (Fig. 2B). To further validate this finding, HA proteins of NC22/17-HA 131△ and NC22/17-HA 131E were expressed using the baculovirus system and the thermal stability of the two HA proteins were measured via the circular dichroism (CD) spectrum, the midpoint transition temperature (Tm) values of NC22/17-HA 131△ and NC22/17-HA 131E

were 58.03 ℃ and 49.89 ℃, respectively (Fig. 2C), indicating NC22/17-HA 131△ has a higher thermostability than NC22/17-HA 131E.

Taken together, clade 2.3.4.4 H5N2, H5N8 and early epidemic H5N6 viruses show similar HA stability to those of clade 2.3.4 avian H5N1 viruses, while the newly emerged HA 131△ H5N6 virus possesses increased HA stability (acidic and thermal), indicating that the point deletion could confer higher infectivity in mammalian hosts.

129 N-Linked glycosylation in hemagglutinin enhanced protein stability

Glycosylation of influenza HA is known to influence immune response and viral properties connected to antigenicity, fusion activity, virulence and receptor-binding specificity (26). AA deletion at HA position 131 could potentially lead to the formation of a new N-linked glycosylation site -NHT- at positions 129–131 (Fig. 3A). To investigate whether this -NHT- site is indeed glycosylated, we first performed electrophoretic analysis of the HA polypeptides of NC22/17-HA 131△ and NC22/17-HA 131E virus treated with or without PNGase F enzyme, which removes all N-linked glycosylation including complex, hybrid and high-mannose type glycans from related proteins. The HA1 polypeptide of NC22/17-HA 131△ exhibited decreased mobility compared with that of NC22/17-HA 131E. However, when the HA1 polypeptides of these two viruses were deglycosylated with PNGase F, they showed similar mobility (Fig. 3B). To further determine the type of N-linked glycosylation, Endo H enzyme was used to trim down high mannose and some hybrid types glycans on viral proteins to a single N-acetylglucosamine. After treatment, both HA proteins migrated similarly; the resistance to Endo H enzyme indicates that the carbohydrate chains of 129 glycosylation site were of a complex type. Mass spectrometry further confirmed that N129 of NC22/17-HA 131△ was glycosylated with a dominant glycoform of HexNAc(5)Hex(5)Fuc(1) (Fig. 3C and 3D). Together, these results confirmed that the amino acid at positions 129-131 in the HA protein of the NC22/17-HA 131△ virus are indeed N-linked glycosylated.

To determine the role of the glycan at position 129, a reverse-genetics derived H5N6 virus NC22/17-HA 131△ with glycan at position 129, and its mutant bearing a T131A mutation with deglycosylation at position 129 were generated. Syncytia formation assays showed that NC22/17-HA 131△ virus effectively mediated syncytia formation at pH 5.5, while the fusion pH of NC22/17-HA T132A virus was higher at 5.7 (SI Appendix, Fig. S5A). NC22/17-HA T132A virus showed a significant decrease in the HA titer after 4 h of incubation and exhibited no HA activity after 8 h. However, HA activity of NC22/17-HA 131△ virus was maintained throughout the entire 14 h of incubation (SI Appendix, Fig. S5B).

These results confirm that glycosylation at position 129 enhanced HA thermal and acid stability.

To further understand the structural basis of 131△ affecting HA stability, we expressed the HA protein of the NC22/17-HA 131△ and NC22/17-HA 131E viruses using a baculovirus expression system and then determined the structures by X-ray crystallography and cryo-electron microscopy (cryo-EM), respectively (Fig. 4A). The HA structure of NC22/17-HA 131△ and NC22/17-HA 131E were solved at resolutions of 2.5 Å and 2.69 Å, respectively (SI Appendix, Table S1, S2 and Fig. S6). Structural analysis found that the deletion of AA at 131 caused the 130-loop to drop by 3.5 Å (Fig. 4B). Insight into the intramolecular force comparison confirmed that the 131△ promote 131T form an additional hydrogen bond with 156T and 157K, respectively, enhancing the force between 130-loop and 150-loop in the RBD region (Fig. 4C). Moreover, an additional glycosylation site was generated on the 130 loop of NC22/17-HA 131Δ due to the deletion of 131E. Electron densities further confirmed that the glycosylation site has good stability (Fig. 4D). However, the orientation of the glycosylation terminal could not be accurately determined due to its flexibility. According to previous studies, sugar modification plays a significant role in the stability of a modified site (27, 28). The curve distance between the glycosylation site and the RBD region was greater than 20 Å, which would not easily cause steric interference with the receptor. Notably, structural analysis shows that the HA trimers of NC22/17-HA 131△ buries larger surface area than NC22/17-HA 131E (12786.2 Å versus 12271.1 Å), indicating that introduction of the N-linked glycosylation at the HA head region raises the compactness of trimeric structure. In summary, we confirm that sugar modification plays a crucial role in enhancing acid and thermal stability of the HA protein of avian H5N6 virus.

Discussion

Since 2013, clade 2.3.4.4 viruses of subtypes H5N2, H5N6 and H5N8 have spread globally with the migration of wild birds causing severe economic losses to the poultry industry (13). Among them, H5N6 subtype virus has frequently been reported to infect a variety of mammals, including 75 human cases (29, 30). The underlying mechanisms responsible for the adaptation of H5N6 virus to mammalian hosts hitherto remains poorly understood. In this study, we showed that a novel N-linked glycosylation site at the head region of HA raised its protein stability in avian H5N6 virus resulting in improved viral replication in mammalian hosts, in particular, along the upper respiratory tract.

HA plays an important role in the attachment of influenza viruses to host cells and, in the process, determines viral host range and pathogenicity. The differences in receptor distribution between humans and avian species are thought to determine the host restriction of influenza A viruses. The weak affinity of AIVs for human-type SAα2,6Gal-linked receptor is considered a key factor for limited human transmissibility (31). Previous studies showed that clade 2.3.4.4 H5Ny viruses, including H5N2, H5N6, and H5N8, have acquired similar affinity for the human-like SAα2,6 Gal-linked receptor (23, 32, 33). Lu *et al.* found that N-linked glycans close to the HA receptor binding domain (RBD) can affect receptor-binding preference through steric hindrance (34, 35). Here we showed that the acquisition of glycosylation on the 130 loop did not affect the receptor-binding properties of H5N6 virus to avian-type and human-type SA receptors. We demonstrated that this glycosylation site is located away from RBD region (>20Å), so as not to affect receptor binding which also suggests that host receptor-binding of H5N6 virus alone cannot account for its relatively frequent infection of mammals.

Upon binding to SA receptor on host cell surface, the virion is internalized by endocytosis. Subsequently, virions are exposed to low endosomal pH and undergo an irreversible conformational change that causes membrane fusion to release the viral genome into the cytoplasm (36, 37). HA is a typical acid-induced class I fusion protein; if the virion is exposed to sufficiently low pH before completion of endocytosis, HA protein is prematurely and irreversibly activated rendering the inactivation of virions (38). The pH of avian respiratory tract is typically between 5.8-6.0, while those of mammalian hosts are relatively lower, at around pH 5.2-5.6 along the human upper respiratory tract (17). An optimal fusion pH is required for balancing viral acidic stability in the mild acidic nasal tissue environment with fusion activation in the acidic endosome. Therefore, viruses adapted to avian hosts usually possess unstable HA at low-pH, and those adapted to mammalian hosts usually possess relatively stable HA at low-pH. In general, human pandemic/epidemic viruses, in particular, have stable HA in the pH range of 5.0 to 5.4 (20), while H5Ny AIVs have relatively high activation pH values that usually ranging from pH 5.6 to 6.0 (39). Herft et al. (2018) demonstrated that the HA of human H5N6 virus A/Guangzhou/39715/2014 exhibited acidic instability (pH 5.6), and therefore presents a low risk to humans (40). Kong et al. (2021) showed that HA G225W attenuated the virulence of H5N6 virus in mice by decreasing acid and thermal stability (41). Here, we showed that H5N2, H5N8 and the earlier epidemic H5N6 virus exhibit activation pH values of 5.7-5.8, whereas the recent H5N6 virus NC22/17, with the AA deletion at position 131 of HA protein, showed lower activation pH of 5.5.

Functionally, we established that improved stability of HA significantly increases H5N6 virus replication in human epithelial cells (*in vitro*), and in mice and ferrets (*in vivo*).

HA stability is influenced by residues located at the RBD, HA1-HA2 interface, spring-loaded HA2 stalk, and the pocket surrounding the hydrophobic fusion peptide (17). Previous research indicated that a key AA residue is one that surrounded by hydrophobic residues (34), forms additional hydrogen bonds (42), or creates salt bridges between structural domains, which in turn impact on HA stability (43). Glycosylation sites have been shown to maintain the stability of viral proteins in dengue virus and SARS-CoV-2 virus (27, 28). Yin et al. (2017) found that the 11N glycosylation site plays a key role in HA cleavage, structural stability and pathogenicity in H5 subtype AIVs (44). In the present study, we found that glycosylation at the head of HA protein increases the surface area of HA trimers resulted in enhanced stability of the trimer structure and reduced the threshold pH for membrane fusion, highlighting the importance of HA protein stability of avian influenza virus in mammalian infection.

Though we confirmed that 131Δ in HA leading to a glycosylation site enhanced the acid and thermo stability of HA that present in 60% of human H5N6 viruses, there are still 40% of viruses do not carry this mutation, 131Δ cannot be fully responsible for the observed association of 2.3.4.4h H5N6 infections. In addition to mutations in HA, mutations in NA and internal genes also play critical roles in host adaptation of AIVs. Mutations can rapidly occur in the HA and PB2 genes of H5N1 AIV during serial passages in ferrets that conferred airborne transmission between ferrets (4). In mouse-adapted H7N9 influenza virus, increased virulence was linked to mutations located in the HA protein and at PB2-E627K (45). Additionally, PB2 R389K substitution could increase H7N9 AIV replication in mammalian cells (46). Genetic analysis found that the internal genes of H5N6 exhibited great evolutionary diversity; in particular, H5N6 virus harboring H9N2 virus internal genes was reported to cause human infection (30). Thus, the extent of contribution of internal genes to the adaptation of H5N6 virus in mammalian hosts will require close scrutiny.

In conclusion, we established that increased acid stability of HA conferred by a novel N-linked glycosylation site at the head of HA protein in prevailing H5N6 viruses is a critical viral determinant for cross-species mammalian host infection. Our findings suggest that continual monitoring of circulating avian influenza viruses for both human-like receptor-binding and acidic HA stability are necessary for pandemic preparedness.

Methods

Ethical compliance.

All animal work was approved by the Beijing Association for Science and Technology (approval SYXK [Beijing] 2007-0023) and conducted in accordance to the Beijing Laboratory Animal Welfare and Ethics guidelines, as issued by the Beijing Administration Committee of Laboratory Animals, and in accordance with the China Agricultural University Institutional Animal Care and Use Committee guidelines (SKLAB-B-2010-003).

Phylogenetic analysis.

All available HA gene sequences of H5Ny (N2, N6, and N8) viruses isolated from different hosts in China from 2010 to 2021 were obtained from Influenza Virus Resource at the National Center for Biotechnology Information (NCBI) (https://www.ncbi.nlm.nih.gov/genomes/FLU/) and Global Initiative on Sharing Avian Influenza Data (GISAID) (https://www.gisaid.org/). Multiple sequence alignment was conducted using MUSCLE v3.7 (47), and maximum likelihood phylogenetic analysis was performed with RAxML (48) via CIPRES Science Gateway (49). One thousand bootstrap replicates were run, and GTRGAMMA + I was used as the nucleotide substitution model. Branch colors and color strips were annotated using iTOL (50).

Viruses and cells.

Four clade 2.3.4.4 H5Ny strains (EC30/10-H5N2, NC08/14-H5N8, EC11/14-H5N6 with HA-131E, and NC22/17-H5N6 with HA 131△, a 2009 pandemic H1N1 virus BJ21/19 and one strain of clade 2.3.4 avian H5N1 virus AH01/06 were previously isolated and kept by our laboratory. Virus stocks were grown in MDCK cells. All experiments with H5 subtype viruses were performed in biosafety level 3 containment.

Human embryonic kidney (HEK293T), adenocarcinomic human alveolar basal epithelial (A549), Madin-Darby Canine Kidney (MDCK), African green monkey kidney (Vero) were cultured with Dulbecco's modified Eagle medium (DMEM; Gibco) supplemented with 10% fetal bovine serum (FBS; Gibco), 100 units/mL penicillin, and 100 μg/mL streptomycin. Primary NHBE cells were obtained from ATCC. Cells of passage 2 were grown on membrane supports (12-mm Transwell-Clear Insert, Corning) at the air-liquid interface in serum-free and hormone- and growth factor-supplemented medium. Fully differentiated 4 to 8-week-old cultures were used for experiments. No trypsin was added to the cultures because previous studies using similar cultures demonstrated efficient proteolytic activation of influenza viruses by endogenous proteases (51, 52).

Generation of recombinant and mutant H5Ny viruses by reverse genetics.

All eight gene segments of NC22/17-H5N6 were amplified by reverse transcription-PCR (RT-PCR) and individually cloned into a dual-promoter plasmid, pHW2000. The reverse genetic virus NC22/17-HA 131△ containing all eight genes from NC22/17, were generated in HEK293T cells as previously described (53). In the backbone of NC22/17, 131E insertion or T131A was introduced into the HA protein by using a QuikChange site-directed mutagenesis kit (Agilent, Santa Clara, CA) according to the manufacturer's instructions, and the remaining seven genes from the NC22/17 virus, were co-transfected into HEK293T cells to generate NC22/17-HA 131E or NC22/17-HA T132A. All viruses were propagated in 9-day-old specific-pathogen-free (SPF) chicken embryos and sequences were verified before use.

Receptor binding assays.

α-2,6 glycans (6'SLN: Neu5Aca2-6Galb1-4GlcNAcb-SpNH-LC-LC-biotin) and α-2,3 glycans (3'SLN: Neu5Aca2-3Galb1-4GlcNAcb-SpNH-LC-LC-biotin) were kindly provided by the Consortium for Functional Glycomics (Scripps Research Institute, Department of Molecular Biology, La Jolla, CA). Receptor-binding specificity was determined by a solid-phase direct binding assay as previously described (54, 55). Briefly, serial dilutions (0.32 μg/ml, 0.63 μg/ml, 1.25 μg/ml, 2.5 μg/ml, 5 μg/ml and 10 μg/ml) of biotinylated glycans 3'SLN and 6'SLN were prepared in PBS, and 100μl of each was added to the wells of the 96-well microtiter plates (Polystyrene Universal-Bind Microplate; Corning) and allowed to attach overnight at 4°C. The plates were then irradiated with 254 nm ultraviolet light for 2 min. After removal of the glycopolymer solution, the plates were blocked with 0.1 ml of PBS containing 2% bovine serum albumin (BSA) at room temperature for 1 h. After washing with ice-cold PBS containing 0.1% Tween 20 (PBST), the plates were incubated in a solution containing influenza virus (64 HA units in PBST) at 4 °C for 12 h. After washing with PBST, chicken antisera were added to each well and the plates were incubated at 4 °C for 12 h. The wells were then washed with ice-cold PBST and incubated with HRP-linked goat-anti-chicken antibody (Sigma-Aldrich) for 2 h at 37°C. After washing with ice-cold PBST, the plates were incubated with O-phenylenediamine in PBS containing 0.01% H_2O_2 for 10 min at room temperature. The reaction was stopped with 0.05 ml of 1 M sulphuric acid and the absorbance was determined at 450 nm.

Virus binding to human tracheal tissues.

The experiment was performed as previously described (55). Briefly, Paraffin-embedded 5 μm sections of normal human tracheal were deparaffinized in xylene and rehydrated by alcohol. Sections were then blocked with 4% BSA in PBS, followed by virus incubation (64 HA units in PBS per section) at 4°C overnight. After four washes in ice-cold PBS, the

sections were incubated with mouse monoclonal antibody specific for influenza nucleoprotein (NP; Abcam, Cambridge, United Kingdom) for 3 h at 4°C. Antibody binding was detected by FITC-labeled goat anti-mouse IgG (Abcam) incubated for 2 h at room temperature. The samples were examined by confocal laser scanning microscopy (Leica Microsystems).

Multistep growth curves on human airway epithelial cells.

NHBE cells were inoculated with virus at an MOI of 0.001. The inoculum was removed after 1 h of incubation at 33°C and replaced with fresh medium. Supernatants were sampled at 12, 24, 36, 48, 60, and 72 hpi, and titrated by inoculating onto MDCK cells. A549 cells were inoculated with virus at an MOI of 0.001. After 1 h of incubation at 37°C, the cells were washed with PBS twice and further incubated with serum-free DMEM. Supernatants were sampled at 12, 24, 36, 48, 60, and 72 hpi, and titrated by inoculating onto MDCK cells. Each experiment was performed in triplicate.

HA acid stability.

HA acid stability was measured using syncytia formation assay as previously described (56). In the syncytia assay, Vero cells in 24-well plates were infected with indicated virus at an MOI of 3. At 16 hpi, infected cells were maintained with pH-adjusted MES buffers ranging from 5.0 to 6.0 for 5 min. After aspiration of pH-adjusted MES, infected cells were incubated with DMEM supplemented with 10% FBS for 3 hr at 37˚C. The cells were then fixed and stained using a Hema 3 Fixative and Solutions (Fisher Scientific). Photomicrographs of cells containing or lacking syncytia were recorded using a light microscope to determine the pH value threshold of membrane fusion.

Thermostability assay.

Viruses were diluted in DMEM and adjusted to 128 HAU/50μL. Virus samples were then incubated at 50℃ for 14 h duration, and HA activities of viruses were measured every 2 h using HA assays with 1% chicken red blood cells.

Deglycosylation using PNGase F or Endo H and Western blot analysis.

Deglycosylation was performed using PNGase F or Endo H enzyme (New England BioLabs, MA, USA) as previously described (57). In brief, virus samples were pre-denatured and then treated with or without the PNGase F for 15min at 50℃ or Endo H enzyme for 1h at 37℃ according to the manufacturer's instructions. Then samples were heated at 100°C for 10 min and then separated on a 10% sodium dodecyl sulfate-polyacrylamide gel electrophoresis (SDS-PAGE) gel, transferred onto a polyvinylidene difluoride (PVDF) membrane (Millipore, USA), and subsequently incubated with a primary antibody specific for H5N1 influenza HA (1:2000, 11689-T54, Sino Biological). The secondary antibody used was horseradish

peroxidase (HRP)-conjugated anti-rabbit IgG (1:10,000, A0208, Beyotime). HRP was detected using a Western Lightning chemiluminescence kit (Amersham Pharmacia, Freiburg, Germany) according to the manufacturer's protocols.

Mass spectrometry analysis of glycopeptides.

Viruses from cell culture supernatants were purified by ultracentrifugation and the virus proteins were separated by SDS-PAGE. Bands of interest were excised, cut into smaller pieces (1 mm × 1 mm), rinsed with water and washed twice in 50 mM ammonium bicarbonate at 37℃ for 30min. The gel pieces were then shrunk in 100 % acetonitrile (ACN) and shaken for 5 min. Solvent was removed, and gel pieces rehydrated in 10 mM DTT in 50 mM AmBic, followed by 40 min incubation at 60 ℃. The gel pieces were again shrunk in 100 % ACN and shaken for 30 min. Solvent was removed, and gel pieces rehydrated in 55 mM iodoacetamide in 50 mM AmBic, followed by 40 min incubation at room temperature. The gel pieces were again shrunk in 100 % ACN and shaken for 15 min. The solvent was removed, gel pieces briefly rinsed with 50 mM AmBic and rehydrated in a small volume (10 μL) of 50 mM AmBic supplemented with LysC-trypsin, chymotrypsin and α-lytic at 37 ℃ for 18 hrs separately follow by PNGase F treatment at 37 ℃ for 4 hrs in O18- water. Peptides were stage-tip purified as previously described, dried, and reconstituted in 10 μL of 0.1 % formic acid prior to analysis (58).

For LC-MS analysis, the peptides were first separated with a Thermo Scientific Ultimate 3000 RSLC nano LC system using trap-elute mode and then emitted into a Thermo Scientific Orbitrap Eclipse mass spectrometer. Solvent A was 0.1% formic acid in water, while solvent B was 0.1% formic acid in 80% acetonitrile. After loading for 3 min with a flow rate of 10 μL/min in the trap column (Thermo Scientific Acclaim PepMap 100 C18, 75μm*2cm, 3μm, 100Å), all of the peptides were further eluted in the analytical column (Thermo Scientific Acclaim PepMap 100 C18, 75μm*25cm, 2μm, 100Å) with a flow rate of 250 nL/min using a gradient of 8% to 30% B for 127 min and 30% to 90% B for 16 min (59). All gradients were followed by a 14 min washing step and a 10 min column equilibration step.

To achieve "on the fly" glycopeptide identification, the HCDpdEThcD method was employed for the data acquisition. The full scan mass spectra were recorded in positive ion mode over a scan range from 350 to 2000 m/z with a 60000 resolut.

Gene cloning, protein expression, and purification.

The sequence encoding the ectodomain of HA from NC22/17-HA 131△ or NC22/17-HA 131E was cloned into the baculovirus transfer vector pFastBac1 (Invitrogen), as previously described (60), in-frame with an N-terminal gp67 signal peptide for secretion, a C-terminal

thrombin cleavage site, a trimerization foldon sequence and a 6× His-tag at the extreme C terminus for purification. Transfection and virus amplification were performed according to the Bac-to-Bac baculovirus expression system manual (Invitrogen). HA protein was produced by infecting suspension cultures of Hi5 cells (Invitrogen) for 2 days. Soluble HA was recovered from the cell supernatants by metal affinity chromatography using a HisTrap HP 5-ml column (GE Healthcare), and purified by ion-exchange chromatography (IEX) using a Mono-Q 4.6/100 PE column (GE Healthcare). As H5 HA consisted of a mixture of uncleaved HA0 and cleaved HA1/HA2, IEX-purified HA was digested with TPCK trypsin (New England Biolabs, 10 mU trypsin/mg HA, overnight at 4°C) to produce uniformly cleaved HA1/HA2, and then purified by gel filtration chromatography using a Superdex-200 10/300 GL column (GE Healthcare) with a running buffer (pH 8.0) of 20 mM Tris-HCl and 50 mM NaCl. The collected protein fractions were concentrated to 10 mg/ml for further use.

Thermostability measurements using CD.

The thermostability of NC22/17-HA 131△ and NC22/17-HA 131E was tested by CD spectroscopy. CD spectra were measured at 20˚C on a Jasco J-810 spectropolarimeter equipped with a water-circulating cell holder (61). Trypsin treated HAs were purified by gel filtration using a running buffer of (20 mmol/L Tris-HCl, 50 mmol/L NaCl, pH 8.0) and diluted into 0.2 mg/mL. CD spectra were measured on a Chirascan spectrometer (Applied Photophysics) using a thermostatically controlled cuvette at temperatures between 20°C and 95°C. Far-UV spectra at 218 nm were collected with a 5 s/point signal averaging and were the accumulation of 5 individual scans; thermal denaturation curves were determined by monitoring the CD value given as the mean residue ellipticity θ_{218} at temperature intervals of 0.5°C at a rate of 1°C/min (62). The actual temperature of the protein solution was measured with a thermistor inserted into the cuvette. The proportion of denatured protein was calculated from the mean residue ellipticity (θ) using the standard method: fraction unfolded (%) = $(\theta-\theta_N)/(\theta_U-\theta_N)$, where θ_N and θ_U are the mean residue ellipticity values in the fully folded and fully unfolded states, respectively. The midpoint transition temperature (Tm) was calculated using the data of denaturation curves in the program Origin 8.0 (OriginLab) (63).

Crystallization, data collection, and structure determination.

The HA protein was crystallized via the sitting-drop vapour diffusion method at 18°C. The NC22/17-HA 131△ HA crystal was grown in a reservoir solution of 0.1 M Tris-HCl pH 8.5, 2.0 M ammonium phosphate monobasic. All crystals were flash-cooled in liquid nitrogen after a brief soaking in reservoir solution with the addition of 20% (v/v) glycerol. X-ray diffraction data were collected at Shanghai Synchrotron Radiation Facility (SSRF) Beamline

BL17U1 (wavelength, 0.97776 Å). All data were processed with HKL-3000 software package (HKL Research) (64). The HA structure was solved by molecular replacement using Phaser (65) from the CCP4 program suite (66). Further rounds of refinement were carried out using the phenix.refine program implemented in the PHENIX package (67) with energy minimization, isotropic ADP refinement, and bulk solvent modeling. The structures were then adjusted using COOT and refined with PHENIX. The stereochemical quality of the final model was assessed with the program PROCHECK (68). The final statistics for data collection and structure refinement are represented in Table S1. Structural illustrations were drawn using PyMOL (https://www.pymol.org).

Cryo-EM sample preparation and data collection.

Aliquots of NC22/17-HA 131E ectodomain (4ul, 0.18mg/ml, in 20 mM Tris pH 8.0, 150 mM NaCl.) were applied to graphene oxide (GO) grids (GO on Quantifoils R1.2/1.3 400 mesh copper grids, R1.2/1.3). In the Vitrobot Mark IV (Thermo Fisher Scientific), the humidity was set at 100%, the protein solution was applied to the grid and there was a wait of 1s before blotting. A blot force of 0 and blot time of 2s were applied to blot the grid after waiting. After blotting, the grid was plunged into precooled liquid ethane at a liquid nitrogen temperature (69).

Images for complex were recorded using FEI Titan Krios microscope (Thermo Fisher Scientific) operating at 300 kV with a Gatan K3 Summit direct electron detector (Gatan Inc) at Shanxi Academy of Advanced Research and Innovation. The automated software (EPU)3 was used to collect 5,746 movies for complex in super-resolution mode at a nominal magnification of 105,000× with a calibrated pixel size of 0.85 Å and at a defocus range between -1.0 and -2.0 um. Each movie has a total accumulate exposure of 60 e-/Å2 fractionated in 32 frames of 1.38 s exposure (70).

Image processing.

The drift correction of all stacks was performed with MotionCor2 (71) and contrast transfer function (CTF) values were calculated with patch CTF estimation implemented in cryoSPARC v.3.3.1. 166,053 particles were picked from a subset of 1,087 micrographs. After 2D classification, ab-initio reconstruction and heterogenous refinement, reference particles from the best volumes were used as a training dataset for the optimization of convolutional neural network in the automated particle picking software Topaz. For the entire dataset, 1,252,539 particles were picked by trained Topaz. The picked particles were then extracted and subjected to reference-free 2D classification. A clean dataset with 1,085,751 particles

from good 2D classes were selected to generate the six initial models, and then subjected to heterogenous refinement. The predominant class containing a subset of 796,965 best particles was subjected to the second round of heterogenous refinement without applying symmetry, and remaining 458,376 particles shows the clear features of secondary structural elements and the high accuracy of particle alignment. These particles were subjected homogenous refinement, which yielded a reconstruction at 2.69 Å resolution. Refer to Supplementary Fig. S6 and Supplementary Table. 2 for details of data collection and processing.

Model building and refinement.

The crystal structure of the HA protein NC22/17-HA 131E was docked into the cryo-EM density maps using CHIMERA (72). The model was manually corrected for local fit in COOT (73) and the sequence register was updated based on alignment. The model was refined against the corresponding map in real space using PHENIX (67), in which the secondary structural restraints and Ramachandran restrains were applied. The stereochemical quality of each model was assessed using MolProbity (74). Statistics for model refinement and validation are shown in Supplementary Table 2.

Mouse challenge studies.

Groups of five 6-week-old female BALB/c mice (Vital River Laboratory) were anesthetized with Zoletil (tiletamine-zolazepam [Virbac], 20μg/g bodyweight) and i.n. inoculated with 50μl virus in 10-fold serial dilutions from 10^7 to 10^5 $TCID_{50}$. The mice in each group were monitored daily for 12 days for weight loss and mortality to determine MLD_{50}. Mice that lost > 25% of their initial body weight were euthanized. MLD_{50} values were calculated according to the Reed and Muench method (75). To monitor virus production, 5 mice infected with 10^6 $TCID_{50}$ virus or PBS from each group were euthanized on 3 and 5 dpi, respectively. Nasal turbinate and lung samples were collected for virus titration and histopathology assay.

Ferret challenge studies.

All 6-month-old male Angora ferrets (Angora LTD), serologically negative for currently circulating influenza viruses (H1, H3, H5, H7, and H9) and > 1.0kg (ranging 1.10 to1.80 kg) in weight, were selected for challenge studies. Ferrets in groups of three were each anesthetized with ketamine (20 mg/kg) and xylazine (1 mg/kg) and i.n. inoculated with 10^6 $TCID_{50}$ of test virus or PBS in a 1-ml volume. The animals were subsequently euthanized on 4 dpi, nasal turbinate, trachea, and lung samples were collected for virus titration and histopathology assay.

Histopathology and immunohistochemistry.

Tissues were fixed in 10% buffered formalin, embedded in paraffin, sectioned, and stained with hematoxylin and eosin (H&E). The tissue sections were also immunostained for viral NP with a monoclonal primary antibody (AA5H; Abcam, Cambridge, United Kingdom). The secondary antibody (Millipore, Billerica, MA, USA) used was conjugated to HRP, and the color reaction was based on the use of an HRP reaction kit (diaminobenzidine tetrahydrochloride; Sigma, St. Louis, MO, USA).

Statistical analysis.

All statistical analyses were performed using GraphPad Prism software version 5.00 (GraphPad Software Inc., San Diego, CA, USA). Statistically significant differences between experimental groups were determined by analysis of variance (ANOVA). Differences were considered statistically significant at a P value of < 0.05.

References

1. Xu X, Subbarao, Cox NJ, & Guo Y (1999) Genetic characterization of the pathogenic influenza A/Goose/Guangdong/1/96 (H5N1) virus: similarity of its hemagglutinin gene to those of H5N1 viruses from the 1997 outbreaks in Hong Kong. *Virology* 261(1):15-19.
2. Surveillance Division of the Communicable Disease Branch of the Centre for Health Protection, Hong Kong SAR, China (2022) Avian Influenza Report.
3. Chen L-M, *et al.* (2012) In vitro evolution of H5N1 avian influenza virus toward human-type receptor specificity. *Virology* 422(1):105-113.
4. Herfst S, *et al.* (2012) Airborne transmission of influenza A/H5N1 virus between ferrets. *Science* 336(6088):1534-1541.
5. Imai M, *et al.* (2012) Experimental adaptation of an influenza H5 HA confers respiratory droplet transmission to a reassortant H5 HA/H1N1 virus in ferrets. *Nature* 486(7403):420-428.
6. Freidl GS, van den Ham H-J, Boni MF, de Bruin E, & Koopmans MPG (2016) Changes in heterosubtypic antibody responses during the first year of the 2009 A(H1N1) influenza pandemic. *Sci Rep* 6:20385-20385.
7. Zhao M, *et al.* (2018) Heterosubtypic Protections against Human-Infecting Avian Influenza Viruses Correlate to Biased Cross-T-Cell Responses. *mBio* 9(4):e01408-01418.
8. Duan L, *et al.* (2008) The development and genetic diversity of H5N1 influenza virus in China, 1996-2006. *Virology* 380(2):243-254.
9. Fan S, *et al.* (2014) A novel highly pathogenic H5N8 avian influenza virus isolated from a wild duck in China. *Influenza Other Respir Viruses* 8(6):646-653.
10. Wu H, *et al.* (2015) Novel reassortant highly pathogenic H5N6 avian influenza viruses in poultry in China. *Infect Genet Evol* 31:64-67.
11. Zhao G, *et al.* (2012) Novel reassortant highly pathogenic H5N2 avian influenza viruses in poultry in China. *PLoS One* 7(9):e46183.
12. Zhao K, *et al.* (2013) Characterization of three H5N5 and one H5N8 highly pathogenic avian influenza viruses in China. *Vet Microbiol* 163(3-4):351-357.
13. Verhagen JH, Herfst S, & Fouchier RAM (2015) Infectious disease. How a virus travels the world. *Science* 347(6222):616-617.

14. Pyankova OG, *et al.* (2021) Isolation of clade 2.3.4.4b A(H5N8), a highly pathogenic avian influenza virus, from a worker during an outbreak on a poultry farm, Russia, December 2020. *Euro Surveill* 26(24).
15. Cao X, Yang F, Wu H, & Xu L (2017) Genetic characterization of novel reassortant H5N6-subtype influenza viruses isolated from cats in eastern China. *Arch Virol* 162(11):3501-3505.
16. Li X, *et al.* (2015) Genetic and biological characterization of two novel reassortant H5N6 swine influenza viruses in mice and chickens. *Infect Genet Evol* 36:462-466.
17. Russell CJ, Hu M, & Okda FA (2018) Influenza Hemagglutinin Protein Stability, Activation, and Pandemic Risk. *Trends Microbiol* 26(10):841-853.
18. de Graaf M & Fouchier RAM (2014) Role of receptor binding specificity in influenza A virus transmission and pathogenesis. *EMBO J* 33(8):823-841.
19. Bullough PA, Hughson FM, Skehel JJ, & Wiley DC (1994) Structure of influenza haemagglutinin at the pH of membrane fusion. *Nature* 371(6492):37-43.
20. Russier M, *et al.* (2016) Molecular requirements for a pandemic influenza virus: An acid-stable hemagglutinin protein. *Proc Natl Acad Sci U S A* 113(6):1636-1641.
21. Castelán-Vega JA, Magaña-Hernández A, Jiménez-Alberto A, & Ribas-Aparicio RM (2014) The hemagglutinin of the influenza A(H1N1)pdm09 is mutating towards stability. *Adv Appl Bioinform Chem* 7:37-44.
22. Imai M & Kawaoka Y (2012) The role of receptor binding specificity in interspecies transmission of influenza viruses. *Curr Opin Virol* 2(2):160-167.
23. Gao R, *et al.* (2018) T160A mutation-induced deglycosylation at site 158 in hemagglutinin is a critical determinant of the dual receptor binding properties of clade 2.3.4.4 H5NX subtype avian influenza viruses. *Vet Microbiol* 217:158-166.
24. Russell CJ (2021) Hemagglutinin Stability and Its Impact on Influenza A Virus Infectivity, Pathogenicity, and Transmissibility in Avians, Mice, Swine, Seals, Ferrets, and Humans. *Viruses* 13(5).
25. Carr CM, Chaudhry C, & Kim PS (1997) Influenza hemagglutinin is spring-loaded by a metastable native conformation. *Proc Natl Acad Sci U S A* 94(26):14306-14313.
26. Kim JI & Park M-S (2012) N-linked glycosylation in the hemagglutinin of influenza A viruses. *Yonsei Med J* 53(5):886-893.
27. Somnuke P, Hauhart RE, Atkinson JP, Diamond MS, & Avirutnan P (2011) N-linked glycosylation of dengue virus NS1 protein modulates secretion, cell-surface expression, hexamer stability, and interactions with human complement. *Virology* 413(2):253-264.
28. Casalino L, *et al.* (2020) Beyond shielding: the roles of glycans in the SARS-CoV-2 spike protein. *ACS Cent Sci* 6(10):1722-1734.
29. Bi Y, *et al.* (2019) Clinical and Immunological Characteristics of Human Infections With H5N6 Avian Influenza Virus. *Clin Infect Dis* 68(7):1100-1109.
30. Bi Y, *et al.* (2016) Genesis, Evolution and Prevalence of H5N6 Avian Influenza Viruses in China. *Cell Host Microbe* 20(6):810-821.
31. Sorrell EM, *et al.* (2011) Predicting 'airborne' influenza viruses: (trans-) mission impossible? *Curr Opin Virol* 1(6):635-642.
32. Guo H, *et al.* (2017) Highly Pathogenic Influenza A(H5Nx) Viruses with Altered H5 Receptor-Binding Specificity. *Emerg Infect Dis* 23(2):220-231.
33. Yamaji R, *et al.* (2020) Pandemic potential of highly pathogenic avian influenza clade 2.3.4.4 A (H5) viruses. *Rev Med Virol* 30(3):e2099.
34. Lu X, *et al.* (2013) Structure and receptor-binding properties of an airborne transmissible avian influenza A virus hemagglutinin H5 (VN1203mut). *Protein Cell* 4(7):502-511.
35. Klenk H-D, Wagner R, Heuer D, & Wolff T (2001) Importance of hemagglutinin glycosylation for the biological functions of influenza virus. *Virus Res* 82(1):73-75.

36. de Vries E, *et al.* (2011) Dissection of the influenza A virus endocytic routes reveals macropinocytosis as an alternative entry pathway. *PLoS Pathog* 7(3):e1001329.
37. Sieczkarski SB & Whittaker GR (2002) Influenza virus can enter and infect cells in the absence of clathrin-mediated endocytosis. *J Virol* 76(20):10455-10464.
38. Skehel JJ & Wiley DC (2000) Receptor binding and membrane fusion in virus entry: the influenza hemagglutinin. *Annu Rev Biochem* 69:531-569.
39. Kaplan BS, *et al.* (2016) Novel highly pathogenic avian A (H5N2) and A (H5N8) influenza viruses of clade 2.3. 4.4 from North America have limited capacity for replication and transmission in mammals. *mSphere* 1(2):e00003-00016.
40. Herfst S, *et al.* (2018) Human clade 2.3.4.4 A/H5N6 influenza virus lacks mammalian adaptation markers and does not transmit via the airborne route between ferrets. *mSphere* 3(1):e00405-00417.
41. Kong X, *et al.* (2021) A single-amino-acid mutation at position 225 in hemagglutinin attenuates H5N6 influenza virus in mice: The 225W in HA attenuates H5N6 virus. *Emerg Microbes Infect* 10(1):2052-2061.
42. Zhang W, *et al.* (2013) An Airborne Transmissible Avian Influenza H5 Hemagglutinin Seen at the Atomic Level. *Science* 340(6139):1463-1467.
43. Rachakonda PS, *et al.* (2007) The relevance of salt bridges for the stability of the influenza virus hemagglutinin. *FASEB J* 21(4):995-1002.
44. Yin Y, *et al.* (2017) Glycosylation at 11Asn on hemagglutinin of H5N1 influenza virus contributes to its biological characteristics. *Vet Res* 48(1):81-81.
45. Qin J, *et al.* (2019) Multiple amino acid substitutions involved in the adaption of three avian-origin H7N9 influenza viruses in mice. *Virol J* 16(1):3.
46. Hu M, *et al.* (2017) PB2 substitutions V598T/I increase the virulence of H7N9 influenza A virus in mammals. *Virology* 501.
47. Edgar RC (2004) MUSCLE: a multiple sequence alignment method with reduced time and space complexity. *BMC Bioinformatics* 5:113.
48. Stamatakis A (2014) RAxML version 8: a tool for phylogenetic analysis and post-analysis of large phylogenies. *Bioinformatics* 30(9):1312-1313.
49. Miller MA, Pfeiffer W, & Schwartz T (2010) Creating the CIPRES Science Gateway for inference of large phylogenetic trees. *2010 gateway computing environments workshop (GCE)*, (Ieee), pp 1-8.
50. Letunic I & Bork P (2019) Interactive Tree Of Life (iTOL) v4: recent updates and new developments. *Nucleic Acids Res* 47(W1):W256-W259.
51. Endo Y, Carroll KN, Ikizler MR, & Wright PF (1996) Growth of influenza A virus in primary, differentiated epithelial cells derived from adenoids. *J Virol* 70(3):2055-2058.
52. Slepushkin VA, Staber PD, Wang G, McCray PB, & Davidson BL (2001) Infection of human airway epithelia with H1N1, H2N2, and H3N2 influenza A virus strains. *Mol Ther* 3(3):395-402.
53. Sun Y, *et al.* (2011) High genetic compatibility and increased pathogenicity of reassortants derived from avian H9N2 and pandemic H1N1/2009 influenza viruses. *Proc Natl Acad Sci U S A* 108(10):4164-4169.
54. Chandrasekaran A, *et al.* (2008) Glycan topology determines human adaptation of avian H5N1 virus hemagglutinin. *Nat Biotechnol* 26(1):107-113.
55. Sun H, *et al.* (2020) Prevalent Eurasian avian-like H1N1 swine influenza virus with 2009 pandemic viral genes facilitating human infection. *Proc Natl Acad Sci U S A* 117(29):17204-17210.
56. Hu J, *et al.* (2022) Mutations in PB2 and HA are crucial for the increased virulence and transmissibility of H1N1 swine influenza virus in mammalian models. *Vet Microbiol* 265:109314.

57. Gao Y, *et al.* (2009) Identification of amino acids in HA and PB2 critical for the transmission of H5N1 avian influenza viruses in a mammalian host. *PLoS Pathog* 5(12):e1000709.
58. Bagdonaite I, *et al.* (2021) Site-Specific O-Glycosylation Analysis of SARS-CoV-2 Spike Protein Produced in Insect and Human Cells. *Viruses* 13(4).
59. Morales-Aparicio JC, *et al.* (2020) The Impacts of Sortase A and the 4'-Phosphopantetheinyl Transferase Homolog Sfp on Streptococcus mutans Extracellular Membrane Vesicle Biogenesis. *Front Microbiol* 11:570219.
60. Zhang W, *et al.* (2013) An airborne transmissible avian influenza H5 hemagglutinin seen at the atomic level. *Science* 340(6139):1463-1467.
61. Zhang N, *et al.* (2011) Crystal structure of swine major histocompatibility complex class I SLA-1 0401 and identification of 2009 pandemic swine-origin influenza A H1N1 virus cytotoxic T lymphocyte epitope peptides. *J Virol* 85(22):11709-11724.
62. Lu X, *et al.* (2013) Structure and receptor-binding properties of an airborne transmissible avian influenza A virus hemagglutinin H5 (VN1203mut). *Protein Cell* 4(7):502-511.
63. Yao S, *et al.* (2016) Structural Illumination of Equine MHC Class I Molecules Highlights Unconventional Epitope Presentation Manner That Is Evolved in Equine Leukocyte Antigen Alleles. *J Immunol* 196(4):1943-1954.
64. Otwinowski Z & Minor W (1997) Processing of X-ray diffraction data collected in oscillation mode. *Methods Enzymol* 276:307-326.
65. Read RJ (2001) Pushing the boundaries of molecular replacement with maximum likelihood. *Acta Crystallogr D Biol Crystallogr* 57(Pt 10):1373-1382.
66. Collaborative CP (1994) The CCP4 suite: programs for protein crystallography. *Acta Crystallogr D Biol Crystallogr* 50(Pt 5):760.
67. Adams PD, *et al.* (2010) PHENIX: a comprehensive Python-based system for macromolecular structure solution. *Acta Crystallogr D Biol Crystallogr* 66(Pt 2):213-221.
68. Laskowski RA, MacArthur MW, Moss DS, & Thornton JM (1993) PROCHECK: a program to check the stereochemical quality of protein structures. *J of Appl Crystallogr* 26(2):283-291.
69. Fan X, *et al.* (2019) Single particle cryo-EM reconstruction of 52 kDa streptavidin at 3.2 Angstrom resolution. *Nat Commun* 10(1):2386.
70. Zhang S, *et al.* (2022) Loss of Spike N370 glycosylation as an important evolutionary event for the enhanced infectivity of SARS-CoV-2. *Cell Res* 32(3):315-318.
71. Zheng SQ, *et al.* (2017) MotionCor2: anisotropic correction of beam-induced motion for improved cryo-electron microscopy. *Nat Methods* 14(4):331-332.
72. Pettersen EF, *et al.* (2004) UCSF Chimera—A visualization system for exploratory research and analysis. *J Comput Chem* 25(13):1605-1612.
73. Emsley P, Lohkamp B, Scott WG, & Cowtan K (2010) Features and development of Coot. *Acta Crystallogr D Biol Crystallogr* 66(Pt 4):486-501.
74. Chen VB, *et al.* (2010) MolProbity: all-atom structure validation for macromolecular crystallography. *Acta Crystallogr D Biol Crystallogr* 66(Pt 1):12-21.
75. Reed L & Muench H (1938) A simple method of estimating fifty percent endpoints. *Am. J. Hygiene* 27:493-497.

Acknowledgments

This work was supported by National Natural Science Foundation of China (32192450, 31873022, 31761133003 and 31870160).

Author contributions

JL, GFG, and HS designed research; HS, HS, JS, WZ, GD, HL, XW, FL, XZ, JL, YB, and YX performed the experiments. XW, JP, YS, QT, YB, and JQ analyzed data; HS, HS, JS, KCC and JL wrote and critiqued the study. All co-authors approved the final version of the manuscript.

Competing interests

The authors declare that they have no competing interests.

Data Availability statement

All data is included in the manuscript and/or supporting information.

Figure legend

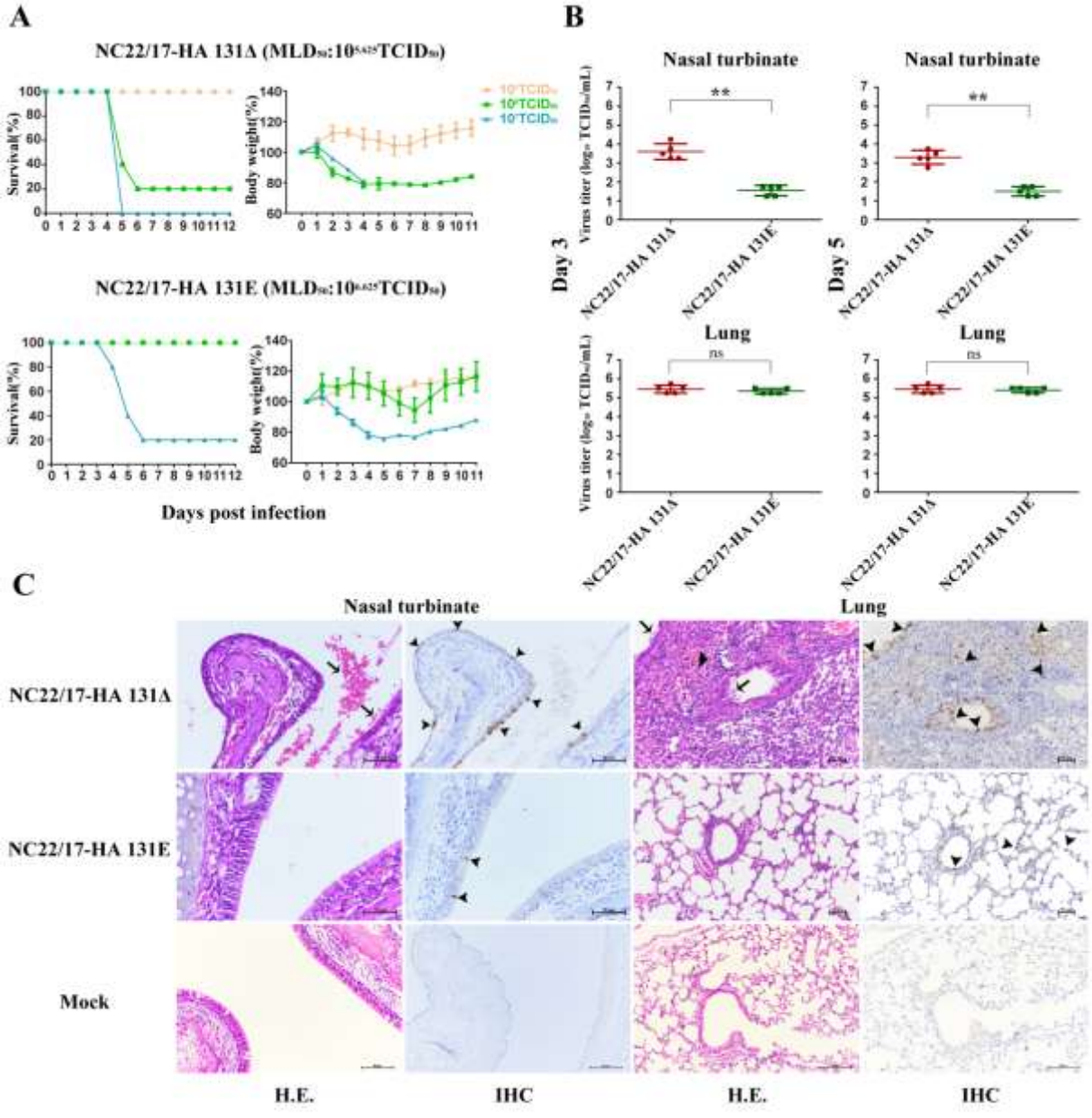

Figure 1. Pathogenicity of H5N6 NC22/17-HA 131△ and NC22/17-HA 131E virus in mice. (A) Weight loss and mortality of mice inoculated with the two different H5N6 rNC22/17 viruses. Six-week-old female BALB/c mice (n = 5 mice/group) were inoculated i.n. with 10^5, 10^6 or 10^7 $TCID_{50}$ of virus. Survival (left panels) and body weight (right panels) were recorded daily. Body weight is presented as means ± SD from live mice. (B) Mice were infected i.n. with 10^6 $TCID_{50}$ of virus, five mice per group were euthanized at 3 and 5 dpi, respectively. Virus titers in nasal turbinates, tracheae and lungs were determined in MDCK cells. Horizontal bars are means (n = 5). Asterisks indicate significant differences in virus titers between the two viruses (* , $P < 0.05$; ** , $P < 0.01$). (C) Representative pathological findings in the nasal turbinates and lungs of mice infected with the indicated viruses at 5 dpi; H & E staining (left panels) and IHC against influenza viral NP antigen (right panels). NC22/17-HA 131E virus-infected mice nasal turbinates appeared normal, with mild bronchitis found in the lungs. NC22/17-HA 131△ virus-infected mice exhibited severe nasal mucosal necrosis and severe peribronchiolitis and bronchopneumonia. Extensive viral NP localization was observed in NC22/17-HA 131△ virus infected nasal turbinates and alveoli (arrows).

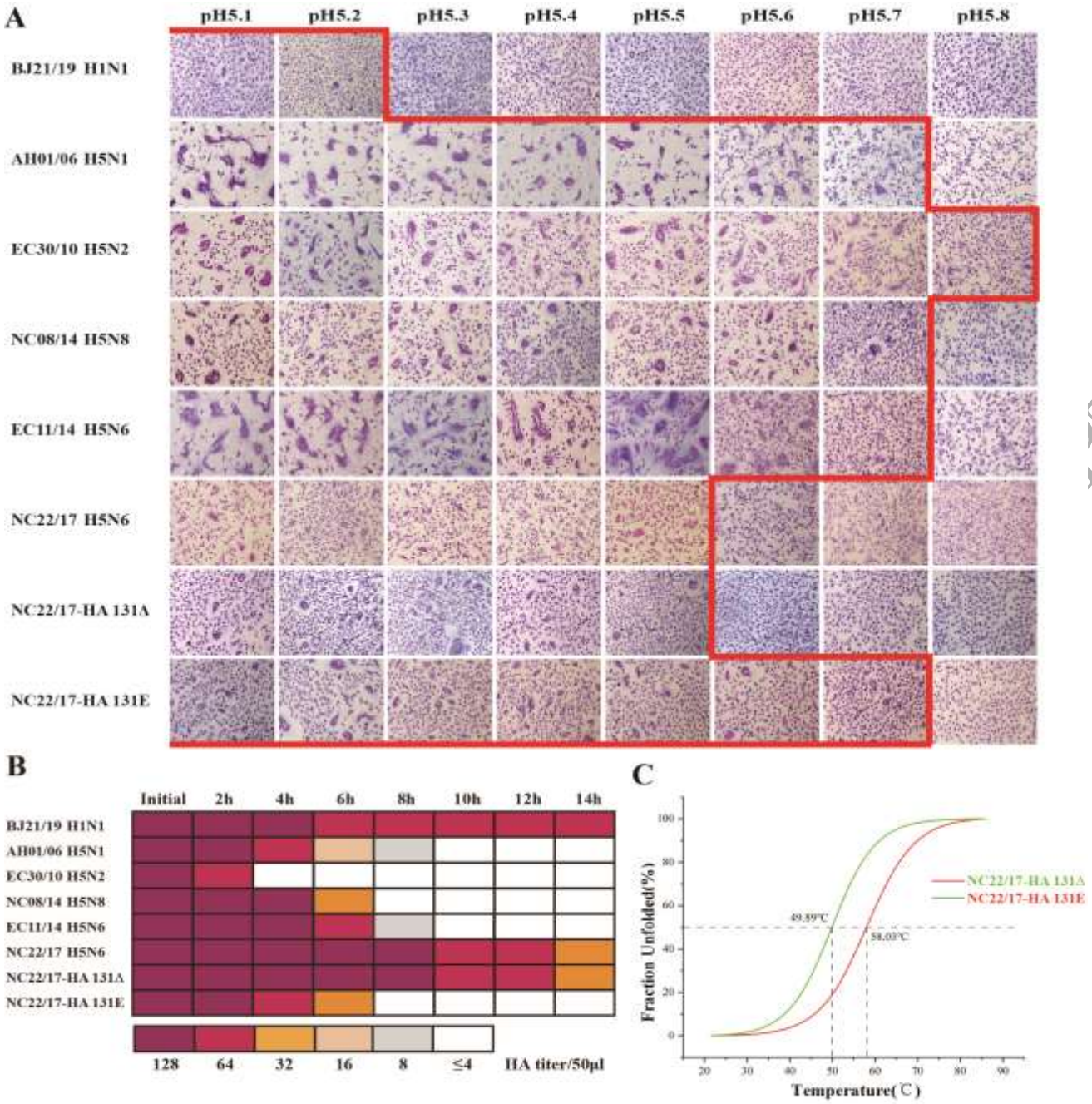

Figure 2. Acid and thermal stability of influenza viruses. (A) pH dependent viral acid stability. Syncytia formation in Vero-E6 cells upon infection with different influenza viruses at different pH values. The red line marks the range of pH values at which fusion was detected microscopically. BJ21/19-H1N1 and AH01/06-H5N1 were included as representative human and avian control viruses, respectively. Three independent experiments were performed; results presented are from one representative experiment. (B) Thermostability of influenza viruses. Viruses were treated at 50°C over a 14-hour time course, and the HA titers were determined at 2 h intervals. Color keys indicate HA titers. Three independent experiments were performed; results presented are from one representative experiment. (C) Thermostability analyses of the NC22/17-

HA 131△ and NC22/17-HA 131E HA proteins. Temperature-dependent CD spectroscopic experiments revealed that the NC22/17-HA 131△ HA protein has higher thermostability.

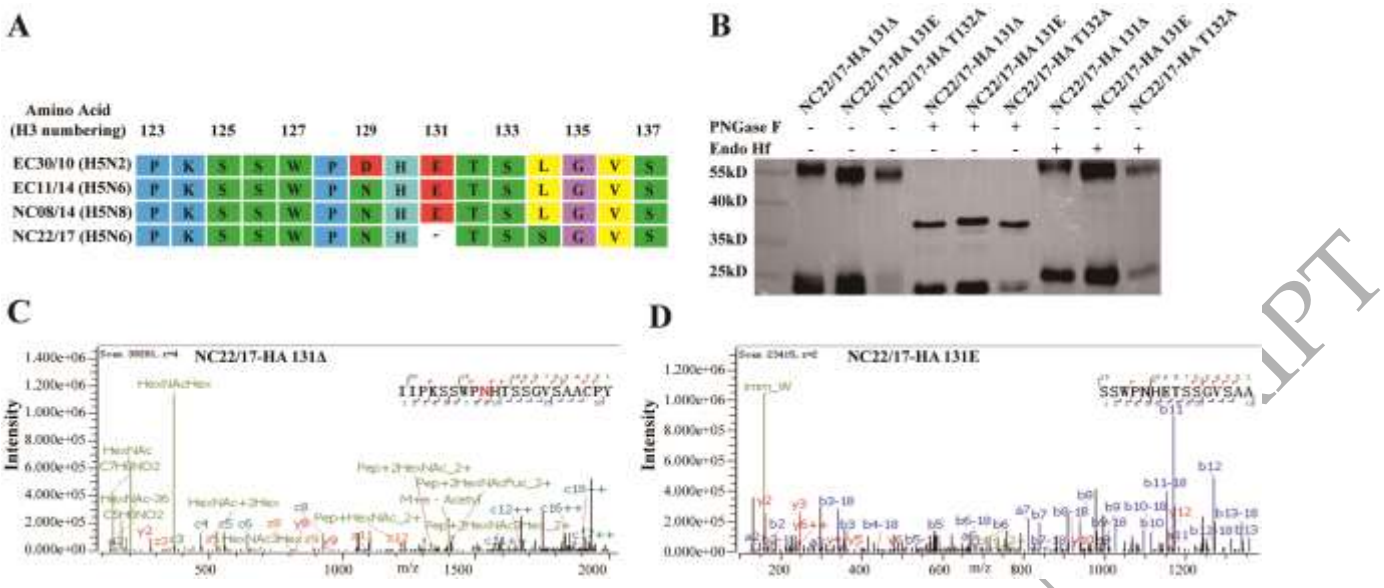

Figure 3. Identification of N-linked glycosylation at position 129 in the HA protein. (A) Amino acid analysis of HA protein of clade 2.3.4.4 H5Ny viruses. The AA deletion at position 131 in the HA protein of H5N6 virus NC22/17 potentially leads to the formation of a N-linked glycosylation site -NHT- at positions 129. (B) Electrophoretic analysis of the HA polypeptides of NC22/17-HA 131△, NC22/17-HA 131E and NC22/17-HA T132A viruses treated with or without PNGase F or Endo H enzyme. The locations of marker proteins are indicated on the left. (C) Mass spectrometry confirmed that NC22/17-HA 131△ HA N129 was glycosylated with a dominant glycoform of HexNAc(5)Hex(5)Fuc(1). (D) No glycan fragment was identified in the NC22/17-HA 131E HA N129 position.

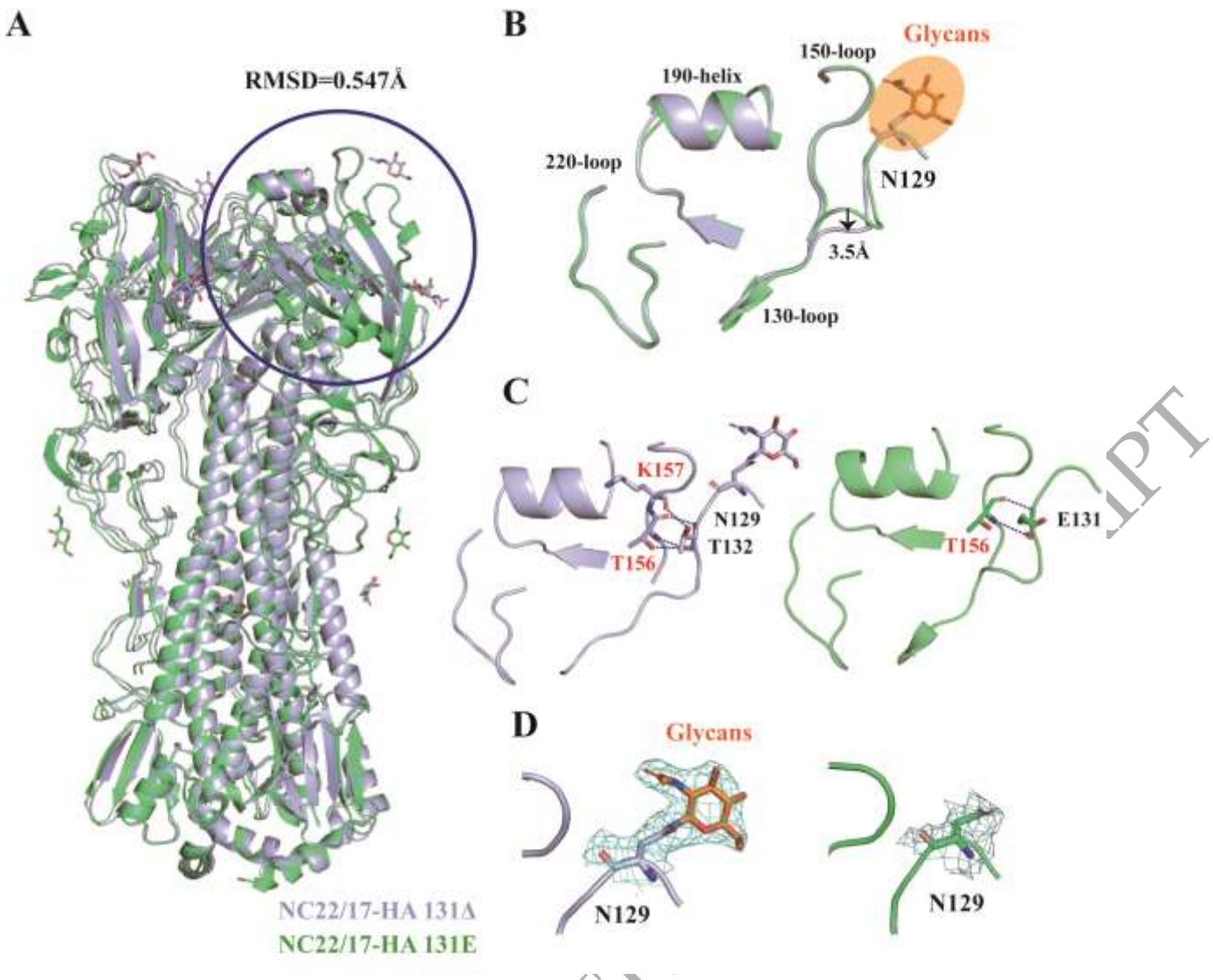

Figure 4. Structural evidence for glycosylation at 130 loop of HA protein. (A) Overall structural alignment of the NC22/17-HA 131 $^{\Delta}$ (light blue) and NC22/17-HA 131E (lime green) HA proteins. (B) Structural comparison of the RBD domains of two HA proteins. Arrows indicate the distance between 130-loops in the two structures. The AA deletion at position 131 in the HA protein formed an additional glycosylation (orange). (C) Changes in the force between 130-loop and 150-loop caused by 131E deletion. The blue dashed lines represent the hydrogen bonding forces between atoms. (D) Comparison of amino acid glycosylation at position 129. Electron densities confirms the presence of amino acid glycosylation in NC22/17-HA 131$^{\Delta}$.